AIAA JOURNAL
Vol. 46, No. 1, January 2008

Turbulent Wake of Rectangular Cylinder Near Plane Wall and Free Surface

M. Agelinchaab,* J. M. Tsikata,* M. F. Tachie,† and K. K. Adane*
University of Manitoba, Winnipeg, Manitoba R3T 5V6, Canada

DOI: 10.2514/1.31933

This paper reports an experimental study of turbulent wake of a two-dimensional rectangular cylinder in a 2500-mm long, 186-mm wide, and 197-mm deep recirculating open channel. The water level upstream of the cylinder was maintained at 100 mm while the aspect and blockage ratios, defined, respectively, as the cylinder's length to thickness and the cylinder thickness to water depth, were 9 and 0.12. The cylinder was mounted across the channel at three different vertical locations: relatively close to the plane wall, close to the free surface, and relatively remote from both the plane wall and the free surface. For each of the preceding three locations, a particle image velocimetry technique was used to conduct detailed measurements at various streamwise–transverse planes around and downstream of the cylinder. For each test condition, the freestream velocity of the approach flow was kept constant at 0.356 m/s. The Reynolds number based on the cylinder thickness was 4270 and the Froude number was 0.36. From these measurements, the streamlines, isocontours of mean vorticity, as well as the mean velocities and turbulent quantities were obtained to document the effects of the plane wall and the free surface on the flow characteristics.

Nomenclature

D	=	thickness of cylinder
$d_{\max}$	=	maximum free surface dip
F	=	Froude number
G	=	gap between lower surface of cylinder and plane wall
H	=	distance from top surface of cylinder to undisturbed free surface
h	=	water depth or channel height
L	=	cylinder length
L_f	=	vortex formation length
L_r	=	length of mean recirculation zone
$l_{\max}$	=	maximum streamwise length of free surface dip
Re_D	=	Reynolds number based on freestream velocity and thickness of cylinder
Re_h	=	Reynolds number based on freestream velocity and depth of flow
U, V	=	streamwise and transverse components of mean velocity
U_e	=	freestream velocity
$U_{\max}$, $U_{\min}$	=	local maximum and minimum values of U
$U_{\max,a}$, $U_{\max,b}$	=	local maximum values of U obtained above and below the wake centerline
$U_{\max,\mathrm{av}}$	=	average of maximum mean velocity above and below wake axis
u, v	=	fluctuating velocity components in streamwise and transverse directions
$u_{\max}$, $v_{\max}$	=	maxima of u and v
$-uv$	=	Reynolds shear stress
x, y, z	=	streamwise, transverse, and spanwise coordinates
Y	=	vertical location above channel wall where cylinder was mounted
δ	=	boundary layer thickness
δ_a	=	y location where $(U_{\max,a}\text{-}U)/(U_{\max,a}\text{-}U_{\min}) = 0.5$
δ_b	=	y location where $(U_{\max,b}\text{-}U)/(U_{\max,b}\text{-}U_{\min}) = 0.5$
Ω_z	=	spanwise mean vorticity

Superscript

$*$	=	normalization by $U_{\max,\mathrm{av}}\text{-}U_{\min}$

I. Introduction

FLUID flows over bluff bodies have diverse and important engineering applications and have been investigated extensively in the past. The vast majority of prior studies were experiments performed behind circular cylinders in an infinite fluid medium. Excellent reviews of earlier articles can be found in [1] by Berger and Wille and Williamson in [2]. A number of studies were performed more recently using direct numerical simulation (DNS) and large eddy simulation (LES) [3]. It is reasonable to assert that the structure and fluid dynamics of turbulent flow past a circular cylinder in an infinite fluid medium are relatively well understood. A number of studies were also conducted to understand the characteristics of turbulent flow past square and rectangular cylinders in an infinite fluid medium [4–6]. Nakagawa et al. [7] studied the turbulent near wake region of square and rectangular cylinders. Their study was conducted for the following four aspect ratios, defined as the ratio of the cylinder length L (in the flow direction) to the thickness D: $L/D = 0.5$, 1, 2, and 3. The blockage ratio, defined as the cylinder thickness (D) to the channel height h was $D/h = 0.2$ in all the experiments. Among others, they concluded that the maxima of streamwise and transverse turbulent intensities ($u_{\max}$ and $v_{\max}$) along the wake centerline occur in the vicinity of the rear stagnation point of the recirculation region. Their results show that the structure of the wake flow depends strongly on L/D.

It is customary to classify the flow downstream of a bluff body into the near wake, intermediate wake, and far wake regions. It is, however, difficult to provide exact boundaries for these regions because the evolution of the flow depends on a variety of geometry and flow parameters such as blockage ratio, end effects, Reynolds number, and freestream turbulence. For circular cylinders, Matsumura and Antonia [8] proposed the following classifications:

Presented as Paper 4478 at the 37th AIAA Fluid Dynamics Conference and Exhibit, Miami, Florida, 25–28 June 2007; received 3 May 2007; revision received 18 July 2007; accepted for publication 29 July 2007.

*Graduate Student, Department of Mechanical and Manufacturing Engineering.

†Associate Professor, Department of Mechanical and Manufacturing Engineering; tachiemf@cc.umanitoba.ca.

very near wake ($x/D \leq 3$), near wake ($3 < x/D \leq 10$), intermediate ($10 < x/D \leq 50$), and far wake ($x/D > 50$). It is generally acknowledged that the very near wake region is dominated by the dynamics of the separated shear layer.

There is also a large body of research on flow past a circular cylinder placed adjacent to a plane wall. Such flows can be used to model many important engineering fluid flow phenomena, for example, underground cables and pipeline on or close to a seabed. It should be noted that the structure of this type of flow is more complex than those found around a cylinder in an infinite medium. For example, the no-slip boundary condition and the associated velocity gradient imposed by the adjacent plane wall produce intense vortical structures that interact with the vortices shed from the bluff bodies. Obviously, the degree of interaction and complications will depend on the cylinder's proximity to the plane wall. One of the first well-known studies to investigate such relatively more complex flows was the flow visualization experiment conducted around a towing circular cylinder in a stationary fluid medium by Taneda [9]. For his experiments, the Reynolds number based on cylinder diameter and towing velocity was $Re_D = 170$. The study was conducted by varying the gap (G) between the lower surface of the cylinder and the plane wall. It was observed that a single row of vortices shed from the cylinder for $G/D = 0.1$ and a regular double row of vortices was shed for $G/D = 0.6$. Price et al. [10] employed flow visualization, particle image velocimetry (PIV), and thermal anemometry to document some of the salient features of flow around a circular cylinder near a plane wall. Their Reynolds number was varied from $Re_D = 1200$ to 4960, and the gap-to-diameter ratio G/D was varied from 0 to 5.0. The authors reported that, for very small G/D, the gap flow is suppressed and separation of the boundary layer occurred both upstream and downstream of the cylinder. The immediate gap ratios ($0.5 < G/D < 0.75$) were characterized by the onset of vortex shedding from the cylinder, and for the largest gap ratios ($G/D > 1$), no separation of the wall boundary layer was observed. Bearman and Zdravkovich [11,12] performed extensive hot-wire measurements and flow visualization in flow past a stationary cylinder. The experiments were conducted for various values of G/D and G/δ, where δ is the boundary layer thickness, and the Reynolds number was varied from $Re_D = 25,000$ to 45,000. Their results and those from other earlier studies [13,14] are vividly summarized by Price et al. [10]. More recently, Dipankar and Sengupta [15] used a numerical technique to study the effects of G/D on lift and gap coefficients.

Flow past circular cylinders placed adjacent to a free surface also has diverse practical applications, for example, offshore structures, submarines, and power generation equipment using tidal power. Compared to classical bluff body flows in an infinite fluid medium, the free surface introduces two additional parameters, namely, Froude number F and gap ratio H/D, where H is the distance from the top surface of the cylinder to the undisturbed free surface [16]. Reichl et al. [16] employed a numerical technique to investigate flow past a circular cylinder close to a free surface for $Re_D = 180$, $0 \leq F \leq 0.7$, and $0.1 \leq H/D \leq 5.0$. The characteristics of shallow turbulent wake in open channels have been studied by Ingram and Chu [17] and Ramachandran [18]. In these studies, the wake generator was mounted on the floor of an open channel, and the goal was to provide insight into the mixing and dilution processes of effluent discharged into shallow water bodies. Balachandar et al. [19] studied the effects of bed friction on the concentration fields in shallow turbulent wakes downstream of a flat plate in open channels. One of the major conclusions from the previous studies was that the Karman vortex streets are annihilated and the spread rate is suppressed if bed friction effects exceed a threshold value. The effects of wall roughness on the development of shallow turbulent wakes have been studied more recently by Tachie and Balachandar [20].

Although the characteristics of turbulent wake downstream of a circular cylinder mounted adjacent to either a plane wall or a free surface have been studied in the past, the effects of a plane wall or a free surface on the characteristics of a turbulent wake downstream of a rectangular cylinder have not yet been investigated in detail. Therefore, the goal of the present study is to investigate the effects of a plane wall and a free surface on the structure and evolution of turbulent wake of a rectangular cylinder in the near and intermediate wake regions in an open channel. A two-dimensional rectangular cylinder with sharp leading and trailing edges was used as the wake generator. The cylinder was placed at three different vertical locations, one at a time: 1) close to the floor of the open channel, 2) close to the free surface, and 3) relatively remote from both the plane wall and the free surface. A PIV was used to conduct detailed velocity measurements in several streamwise–transverse (x–y) planes. The instantaneous and ensemble-averaged flow patterns as well as mean and turbulent statistics at selected locations were obtained to document the salient features of the flow. The data sets presented in this study will also be useful for validating turbulence models.

II. Experimental Setup and Measurement Procedure

A. Experimental Setup

The experiments were performed in a recirculating open channel having a test section that was 2500 mm long, 200 mm wide, and 200 mm deep. The side and bottom walls of the channel were made of clear acrylic to facilitate PIV measurements. A two-dimensional acrylic rectangular cylinder with sharp leading and trailing edges was used to generate the wakes. The length and width of the rectangular cylinder were, respectively, $L = 110$ mm and $W = 186$ mm, whereas the nominal thickness provided by the supplier of the acrylic plate was $D = 12$ mm so that $L/D \approx 9$. Vernier callipers were used to measure the thickness of the bar at 30 randomly selected locations along the cylinder, D_x and then across the cylinder, D_z. The mean values were found to be $D_x = 11.8$ mm and $D_z = 11.7$ mm, whereas the corresponding standard deviations were $\sigma_x = 0.21$ mm and $\sigma_z = 0.09$ mm. A provisional test section made from a 6-mm acrylic plate was inserted into the main channel to hold the cylinder in place. The insert was 2500 mm long, 188 mm wide, and 197 mm deep, and its base was tightly screwed onto the floor of the main channel.

Figure 1 shows a schematic diagram of the top and side views of the inserted test section, and also defines some of the flow nomenclature and the Cartesian coordinate system used. Figure 1c also shows sketches of the mean velocity profile of the approach boundary layer as well as profiles on and downstream of the cylinder. As shown, x, y, and z are, respectively, in the streamwise, transverse, and spanwise directions; $x = 0$ at the rear or trailing edge of the cylinder which is located 1310 mm downstream of the inlet to the test section, $y = 0$ coincides with the midthickness of the plate, $z = 0$ at the midplane of the channel, $x' = 0$ is at the leading edge of the cylinder which is located at 1200 mm downstream of the inlet to the test section, and y' is at the surface of the plane wall. The water level was maintained constant at $h = 100$ mm in all the experiments. The blockage, defined as the cylinder thickness to water depth, was $D/h = 0.12$. The cylinder was mounted at three different vertical locations, $Y = 20$, 40, and 60 mm (one at a time) relative to the floor of the channel by screwing it onto the side walls of the inserted channel at $x' = 55$ mm (see Fig. 1). This produced gap-to-thickness ratios of $G/D = 1.2$, 2.8, and 4.5 relative to the floor of the inserted channel while the corresponding values of the ratio H/D (where H is the distance between the upper surface of the cylinder to the undisturbed free surface) were $H/D = 6.2$, 4.5, and 2.8. Note that the origin of y (relative to the plane wall or channel floor) changes with G/D. The volume flow rate and approach velocity were maintained constant to ensure a similar approach flow in all the experiments. The approach boundary layer was tripped using sanding mesh as shown in Fig. 1. With the cylinder mounted in the test section, it was observed that the free surface around the cylinder dipped below the undisturbed free surface upstream of the cylinder. This is indicated by the dashed line close to the free surface in Figs. 1b and 1c, and the dependence of this depression on G/D will be discussed subsequently. As will be shown later, the local maxima of U above and below the wake axis are not always identical because of the cylinder's proximity to the plane wall or free surface. These local maxima above and below the wake axis are denoted by $U_{\max,a}$ and $U_{\max,b}$, respectively, in Fig. 1c while the corresponding wake

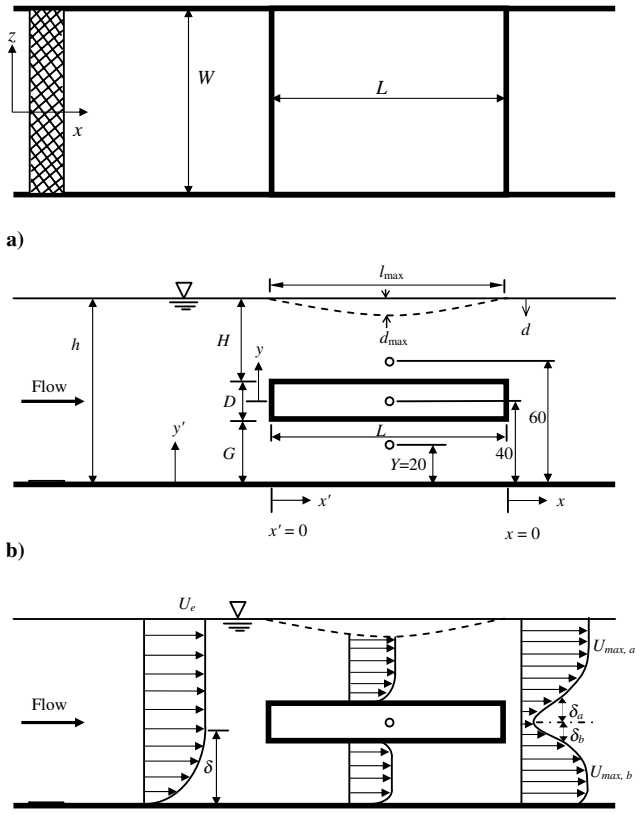

Fig. 1 Schematic diagram of top view a), and side views b) and (c) of the inserted test section that also serves to define the flow nomenclature and the Cartesian coordinate system used.

half-widths are denoted by δ_a and δ_b. The exact definitions of δ_a and δ_b will be provided in a later section.

B. PIV System

A PIV technique was used to conduct the velocity measurements. The flow was seeded with 5 μm polyamide seeding particles whose specific gravity was 1.03. An Nd-YAG, 120 mJ/pulse laser of 532 nm wavelength was used to illuminate the flowfield. The laser sheet was located at the midplane of the channel. A 12-bit high-resolution digital camera (Dantec Dynamic HiSense 4M camera) that uses a charge-coupled device (CCD) with 2048×2048 pixels and has a 7.4 μm pixel pitch was used to image the flowfield. The measurements were made at a field of view of 95×95 mm, the particle image diameter was 15 μm (2 pixels), and the sampling rate was 5.8 Hz. The particle settling velocity and response time were, respectively, 4.1×10^{-4} μm/s and 1.43 μs. The instantaneous images were processed using the adaptive correlation option of FlowManager (version 4.50.17) developed by Dantec Dynamics. A 32×16 pixels interrogation window (IW) with 50% overlap and moving average validation was used. The adaptive correlation uses a multipass fast Fourier transform (FFT) cross-correlation algorithm to determine the average particle displacement within the IW. A three-point Gaussian curve fit was employed to determine particle displacement with subpixel accuracy. The mean velocity and turbulent statistics were calculated using a MATLAB script developed in our laboratory, and based on preliminary convergence tests, it was decided to use 2000 instantaneous image pairs to compute the mean velocity and turbulent statistics reported subsequently.

C. Measurement Uncertainty

Uncertainty analysis was made following the AIAA standard derived and explained by Coleman and Steele [21]. In general, a complete uncertainty analysis involves identifying and quantifying both the bias and precision errors in each part of the measurement chain. In a PIV technique, the accuracy of the velocity measurement is limited by the accuracy of the subpixel interpolation of the displacement correlation peak. Other sources of measurement uncertainties include particle response to fluid motion, light sheet positioning, light pulse timing, and size of interrogation area. Detailed analyses of bias and precision errors inherent in the PIV technique are available in Prasad et al. [22] and Forliti et al. [23]. Forliti et al. [23] showed that a Gaussian peak-fitting algorithm has the lowest bias and precision errors. On the basis of the size of the interrogation area and curve fitting algorithm used to calculate the instantaneous vector maps, and the large number of instantaneous images used to calculate the mean velocity and turbulent statistics, the uncertainty in the mean velocities at 95% confidence level was estimated to be $\pm 2\%$. The uncertainties in turbulence intensities and Reynolds shear stress are estimated to be $\pm 6\%$ and $\pm 10\%$ of the peak values. Close to the plane wall and the rectangular cylinder, uncertainties in mean velocities and Reynolds stresses are estimated to be ± 2.5 and $\pm 12.5\%$, respectively.

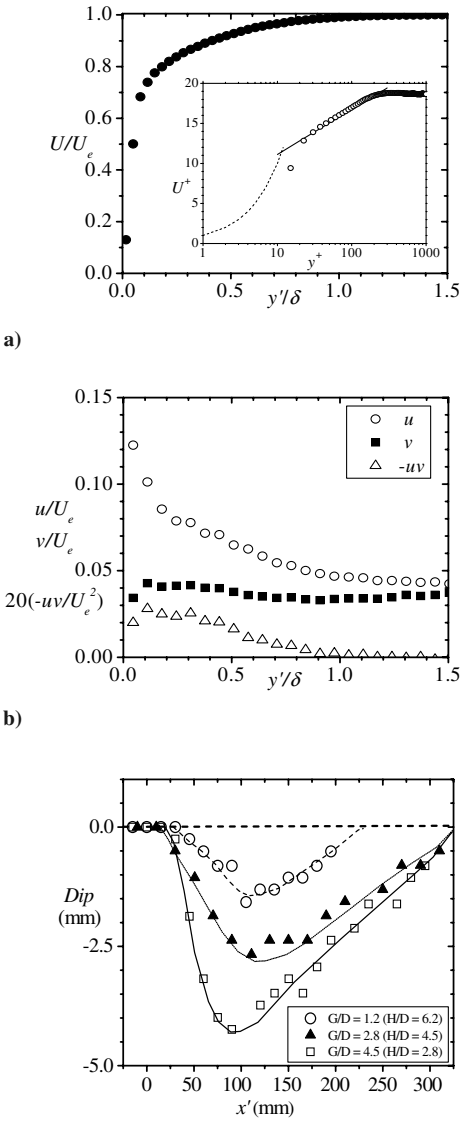

Fig. 2 Mean velocity distribution in outer and inner coordinates a), the dashed line is the law of the wall, $U^+ = y^+$ and the solid line is the log law, $U^+ = 2.44\,\ell n\, y^+ + 5.0$; turbulent intensities and Reynolds shear stress b); and dip in the free surface close to the cylinder for the three gap ratios c), the dashed line is drawn with reference to the free surface upstream of cylinder, and the other lines through the symbols are for visual aid only.

D. Flow Qualification

Before conducting measurements around and downstream of the cylinder, measurements were obtained at $x'/D = -25$ (i.e., upstream of the leading edge of the cylinder) to characterize the nature of the approach flow. The freestream velocity was $U_e = 0.356$ m/s while the Reynolds numbers based on depth of flow and cylinder thickness were, respectively, $Re_h = 35,600$ and $Re_D = 4270$, and the Froude number was $F = 0.36$. The approach flow was, therefore, in turbulent and subcritical regimes. The mean velocity distributions in outer and inner coordinates are shown in Fig. 2a while the turbulent intensities and Reynolds shear stress are shown in Fig. 2b. These profiles are similar to previous laser Doppler anemometry (LDA) and PIV measurements in open channel flows [24,25]. The boundary layer thickness, defined as the y location where $U/U_e = 0.99$, was $\delta = 12$ mm, and so the mean velocity is uniform across the outer 88% of the water depth. The background turbulence level close to the free surface was $u/U_e = 0.04$ which is an order of magnitude higher than typical values reported in wind-tunnel experiments.

It was observed that the approach flow was substantially distorted by the presence of the cylinder, and the degree of distortion varied with the gap ratio. As an example, Fig. 2c shows the dip in the free surface close to the cylinder (relative to the undisturbed free surface) for the three different gap ratios. Note that $x' = 0$ corresponds to the leading edge of the cylinder. The dip is larger and extends over a longer streamwise distance when the cylinder is mounted closest to the free surface. For example, with the cylinder closest to the plane wall ($G/D = 1.2$, $H/D = 6.2$), the maximum dip was $d_{\max} = 1.2$ mm and it extended a streamwise distance of $l_{\max} = 200$ mm. When the cylinder is mounted closest to the free surface ($G/D = 4.5$, $H/D = 2.8$), the corresponding values are $d_{\max} = 4.3$ mm and

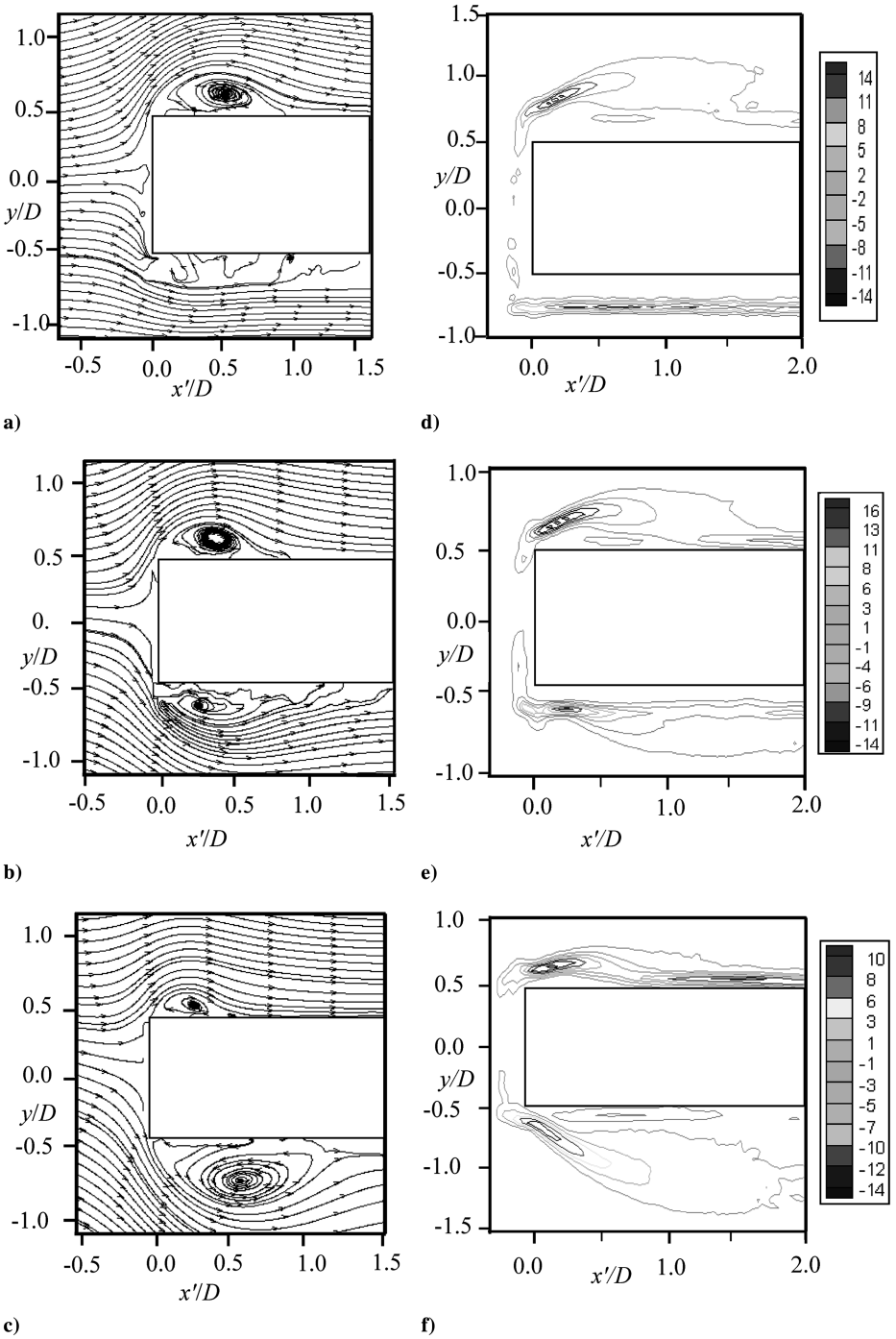

Fig. 3 Streamlines a)–c) and isocontours of the mean vorticities d)–f) close the leading edge of the cylinder. a), d): $G/D = 1.2$; b), e): $G/D = 2.8$; and c), f): $G/D = 4.5$.

$l_{max} = 300$ mm. The implications of this observation for the development of the wake will be discussed subsequently.

III. Results and Discussion

A. Streamlines and Isocontours of Mean Vorticity

The streamlines and isocontours of spanwise vorticity ($\Omega_z = \partial V/\partial x - \partial U/\partial y$) were obtained to reveal some of the qualitative features of the mean flow pattern close to the leading edge (Fig. 3) and the trailing edge (Fig. 4) of the cylinder. The vorticity is made dimensionless using the approach freestream velocity ($U_e = 0.356$ m/s) and the cylinder thickness ($D = 0.012$ m). The approximate location of the cylinder is shown in each figure. The vorticity is predominantly negative above the cylinder and positive beneath it which is in accordance with the orientation of the shear layer. The streamlines shown in Figs. 3b and 3c revealed that, for $G/D = 2.8$ and 4.5, two distinct vortices are formed close to the leading edge: a clockwise rotating vortex above the cylinder and a counterclockwise rotating vortex beneath it. When the cylinder is mounted close to the plane wall ($G/D = 1.2$), a well-defined clockwise rotating vortex is also observed above the cylinder but no distinct vortex was found below the cylinder. The quality of the images in the gap between the plane wall and the cylinder for $G/D = 1.2$ is somehow compromised, and it is not clear if the lack of vortex below the cylinder for $G/D = 1.2$ is due to poor quality of the images or if it is annihilated by the plane wall. The size of the vortices formed above the cylinder is largest for the smallest gap ratio (Fig. 3a) and smallest for the largest gap ratio (Fig. 3c). On the other hand, the size of the vortices below the cylinder increases with the gap ratio. It should be noted that the vortices below and above the cylinder for the intermediate gap ratio are nearly similar in size. Similar to the streamlines, for the largest gap ratio, the vortex above the cylinder is shallower than that formed beneath it (Fig. 3f), while the reverse is true for the smallest gap ratio (Fig. 3d). It appears, therefore, that the plane wall and free surface have the same qualitative effects of the mean flow patterns close to the leading edge; that is, the plane wall tends to suppress the lower vortices when the cylinder is mounted close to the wall while the free surface suppresses the upper vortices when the cylinder is mounted close to the free surface. A salient feature of cylinders with large L/D is the

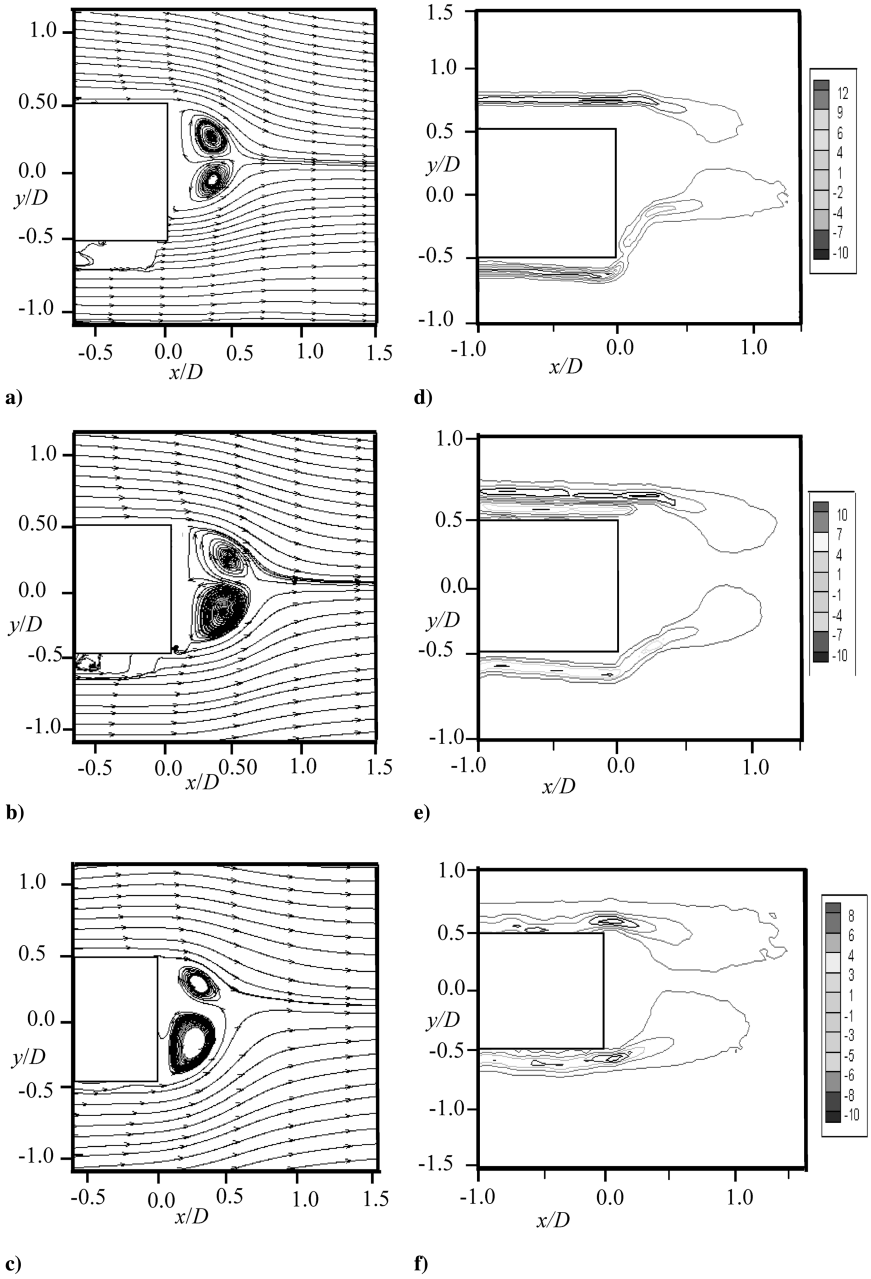

Fig. 4 Streamlines a)–c) and isocontours of the mean vorticities d)–f) close the trailing edge of the cylinder. a), d): $G/D = 1.2$; b), e): $G/D = 2.8$; and c), f): $G/D = 4.5$.

observation that the vortices that are shed at the leading edge periodically reattach on the bottom and top surfaces of the cylinder [7]. Similar observations were made in the experimental study by Taniguchi and Miyakoshi [13] and in the DNS study by Hermann et al. [26] over arrays of a rectangular cylinder with $L/D = 10$. The instantaneous vorticity contours obtained in the present study (not shown) are in general agreement with prior results.

For all three gap ratios, two counter-rotating vortices are observed at the trailing edge. It is evident that, for the largest gap ratio (Fig. 4c), the lower counter-rotating vortex is larger than the clockwise rotating vortex above the cylinder while the pair of vortices for the immediate and smallest G/D values are approximately similar in size. The peak vorticity is nearly the same for the three gap ratios but those found at the trailing edge are smaller than the corresponding leading edge values. It is also important to note that, as the flow exits the relatively narrow gap between the cylinder and the plane wall for $G/D = 1.2$ and 2.8, the vortex is "sucked" upward from the plane wall.

B. Shear Layers Close to Plane Wall and Free Surface

When a cylinder is placed in an infinite fluid medium, the wake flow will evolve free from any interference from a solid boundary or a free surface. As observed earlier, however, the flow patterns in this study are somewhat modified by the proximity of the cylinder to the plane wall or the free surface. To complement the earlier observations, plots of the mean velocity and turbulent intensity profiles were used to reveal the effects of the plane wall on the shear

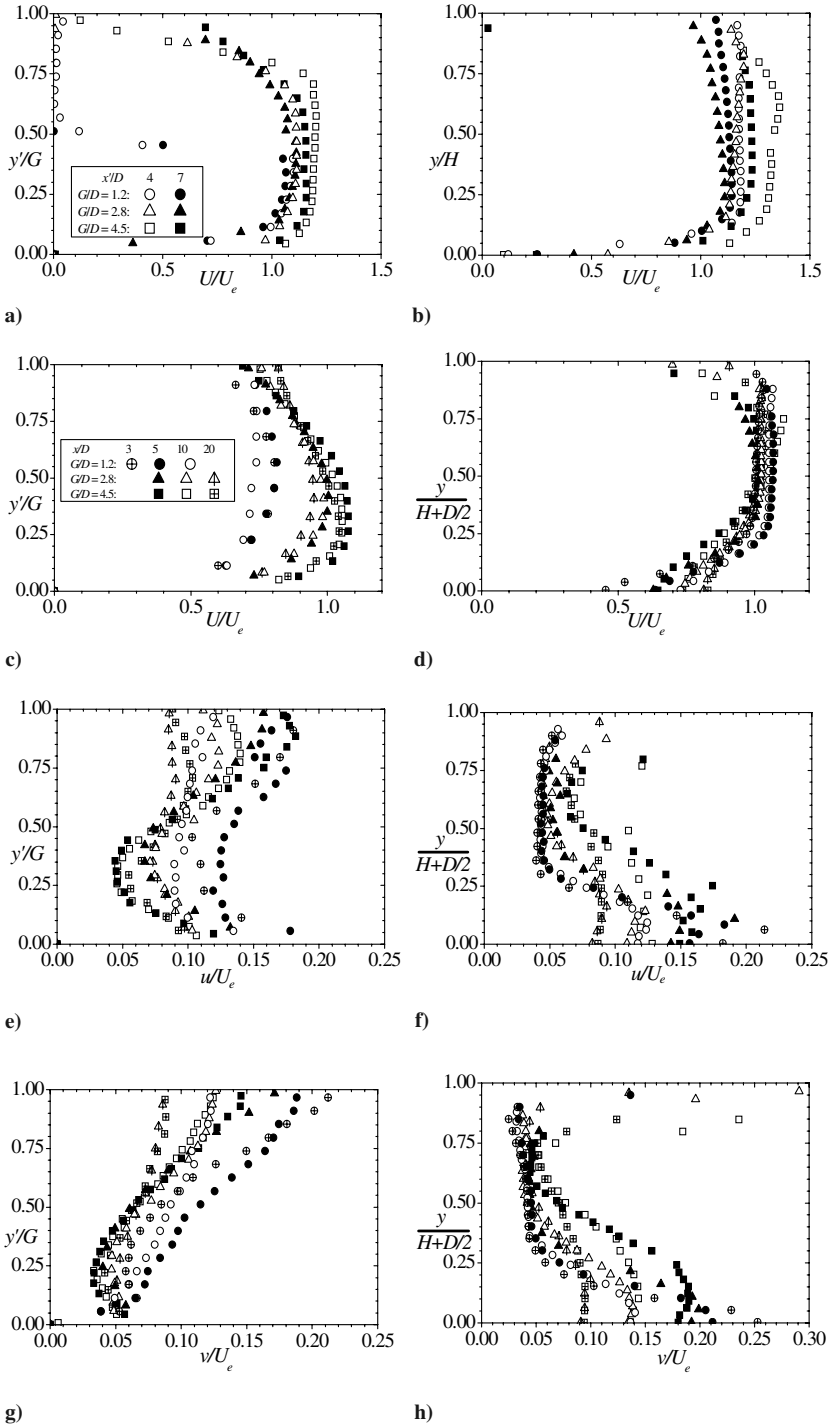

Fig. 5 Mean velocity and turbulent intensities developed between the lower surface of the cylinder and the plane wall a), c), e), and g); and upper surface of cylinder and the free surface b), d), f), and h).

layer that developed between the lower surface of the cylinder and the plane wall (referred to as the lower shear layer, LSL). Similar plots were obtained to study free surface effects on the shear layer that developed between the top surface of the cylinder and the free surface (referred to as the upper shear layer, USL). The mean streamwise velocity profiles obtained around the cylinder at $x'/D = 4$ and 7 for the LSL and USL are plotted, respectively, in Figs. 5a and 5b. All velocities are normalized by $U_e = 0.356$ m/s, and it should be noted that, for the LSL (Fig. 5a), y' is measured relative to the plane wall and normalized by G while for the USL (Fig. 5b), y is measured relative to the upper surface of the cylinder and normalized by H. When the cylinder was mounted close to the plane wall ($G/D = 1.2$), U is nearly zero across the upper half of the LSL (Fig. 5a). The blockage produced by the cylinder increased the local maximum of U compared to the approach freestream velocity (Fig. 5a). The profiles for the USL resemble those obtained in classical open channel flows. However, significant distortion produced by depression in free surface (as documented in Fig. 2c) can be observed in the outer regions of the USL profiles for $G/D = 2.8$ and 4.5 (Fig. 5b). The substantial dip and concomitant flow acceleration around the cylinder for $G/D = 4.5$ produced local values of U that are typically 10 to 40% higher than the approach velocity.

The profiles of mean velocity and turbulent intensities at $x/D = 3$, 5, 10, and 20 are shown in Figs. 5c–5h to demonstrate the subsequent downstream development of the LSL and USL. Note that x is measured relative to the trailing edge of the cylinder. For the USL profiles shown in Figs. 5d, 5f, and 5h, y is measured relative to the wake axis and normalized by the distance from the wake axis to the free surface ($H + D/2$). The effects of the plane wall are evident in the lower half of the profiles plotted in Figs. 5c, 5e, and 5g. These effects include a substantial decrease in the mean velocity outside the wake of $G/D = 1.2$ below the approach freestream velocity. This is likely caused by an intense interaction between the vortical structures produced by the strong shear generated by the plane wall and the vortices shed from the bluff bodies. In contrast to wake flow in an infinite medium, it is observed that the local value of $U_{\max}$ tends to decrease with increasing streamwise distance even for a given gap ratio. For $G/D = 1.2$, U remains flat into the wake region, an indication that the plane wall annihilated the lower wake region a short distance downstream of the cylinder. The turbulent intensities decreased outside the wake region but increased as the plane wall is approached. In some cases, the near-wall peak values of u are higher than those found in the wake region.

For the upper shear layer, it is observed that U remains nearly uniform outside the wake region with a few exceptions (which correspond to a region of significant dip of the free surface). Outside the wake region, values of U are typically larger when the cylinder is mounted close to the free surface (i.e., for $G/D = 4.5$) than for the other two (smaller) gap ratios. Close to the free surface, the turbulence levels are substantially high (typically 5 to 10% of U_e) and in general, the background turbulence levels outside the wake region are also higher for $G/D = 4.5$. As expected, Fig. 5 demonstrates that the most significant effects of the plane wall are observed in the lower shear layers for the smallest gap ratio ($G/D = 1.2$), and it appears that the effects of the free surface are minimal for $G/D = 1.2$ compared to $G/D = 2.8$ and 4.5.

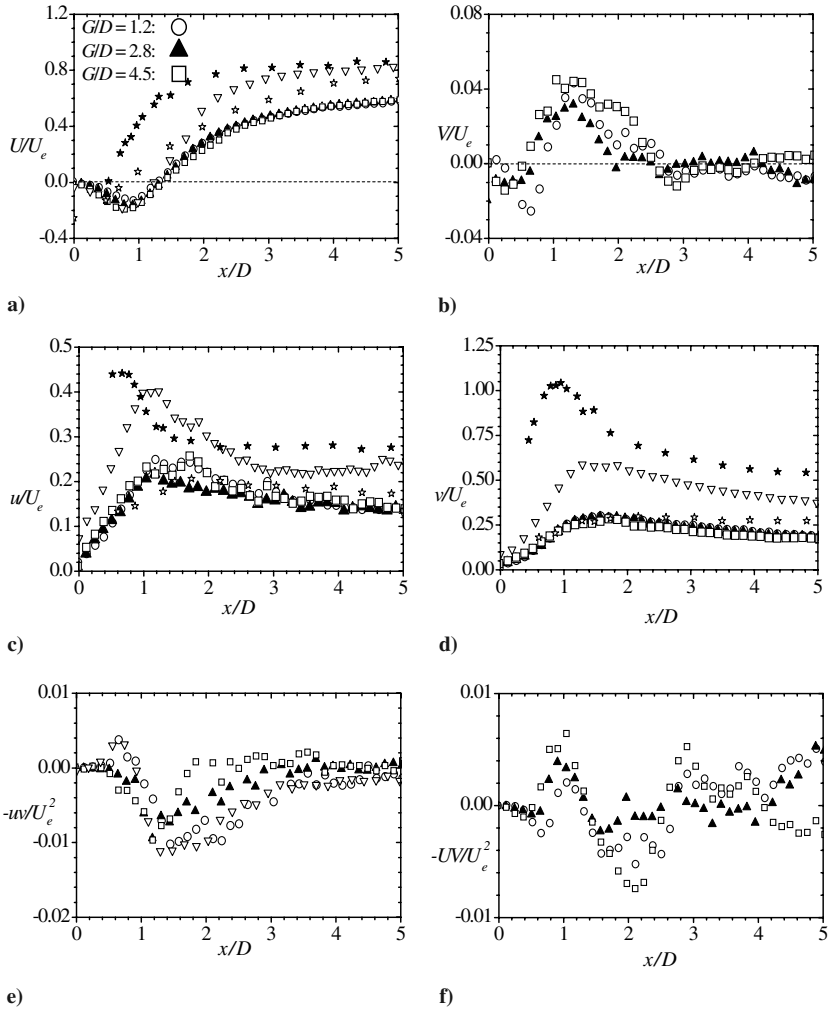

Fig. 6 Mean velocities a) streamwise and b) transverse; and turbulent quantities c) streamwise intensities, and d) transverse turbulent intensities; turbulent momentum flux e); and mean momentum flux f) along the wake axis. ▽: data from Paul [27]; ★: data from Nagakawa et al. [7] for $L/D = 1$; ☆: data from Nagakawa et al. [7] for $L/D = 2$.

C. Wake Flow

1. Mean Velocities and Turbulent Quantities Along the Wake Axis

Figure 6 shows the distributions of the mean velocities, turbulent intensities, and both the mean and turbulent momentum fluxes along the wake axis, $y = 0$. Corresponding data for a circular cylinder [27] are shown for comparison. Note that, for the circular cylinder, $x = 0$ at its rear. As noted earlier, Nakagawa et al. [7] conducted measurements in the wake of rectangular cylinders for which $L/D = 0.5$, 1, 2, and 3. Their data sets for $L/D = 1$ and 2 are also shown in Fig. 6. Figure 6a shows that the gap ratio has a noticeable effect on $(U/U_e)_{\min}$. For example, $(U/U_e)_{\min}$ varied from -0.12 for $G/D = 1.2$ to -0.16 for $G/D = 2.8$, and -0.19 for $G/D = 4.5$. This implies that the plane wall decreased the magnitude of $(U/U_e)_{\min}$ by 25% compared to the value measured for the intermediate cylinder location, whereas the free surface increased the magnitude of $(U/U_e)_{\min}$ by about 20%. The $(U/U_e)_{\min}$ value obtained for $G/D = 4.5$ is not markedly different from $(U/U_e)_{\min} = -0.18$ reported for a circular cylinder but it is significantly different from $(U/U_e)_{\min} = -0.25$ for a rectangular cylinder with $L/D = 2$. The mean velocity recovered more slowly in the present study than for the circular and square cylinders but the recovery behind the rectangular cylinder with $L/D = 2$ is slower in the intermediate wake region.

Figure 6b shows that the maximum value of V/U_e rose to about 4% at $x/D \approx 1.4$, which corresponds approximately to the downstream edge of the recirculation zone. The turbulent intensities and the Reynolds shear stress increase rapidly along the wake axis to a maximum followed by a gradual decay. The mean and turbulent momentum fluxes are of the same order of magnitude. The large values of u/U_e and v/U_e in the near wake region can be attributed to the alternate vortex shedding from the cylinder, and it is evident that the present values of u/U_e and v/U_e are comparable to those reported behind the rectangular cylinder with $L/D = 2$ but are substantially lower than those measured behind the circular and square cylinders. For example, $(u/U_e)_{\max}$ is approximately 20 to 25% in the present study compared to 40 and 44% in the circular and square cylinder wakes, while $(v/U_e)_{\max}$ is about 28% in the present study and 58 and 100% in the circular and square cylinder wakes, respectively. These results show that the transverse turbulent intensity is substantially higher than the streamwise turbulent intensity. The ratio $v_{\max}/u_{\max}$ is only 1.25 in the present study compared to 1.5 and 2.0, respectively, for the circular and square cylinders.

The length of the mean recirculation zone, defined as the distance between the trailing edge of the cylinder and the downstream location where $U/U_e = 0$ (Fig. 6a), is found to be $L_r/D \approx 1.3$ for all three gap ratios studied in the present work. This value is not significantly different from a value of 1.2 for the circular cylinder [27]. Nakagawa et al. [7] reported a value of $L_r/D = 0.6$ for a square cylinder and $L_r/D = 1.8$ and 0.9, respectively, for rectangular cylinders of $L/D = 2$ and 3. As noted earlier, for large values of L/D, the separated shear layers at the leading edges reattached periodically on the lower and upper surfaces of the cylinder. These may partly explain the disparities observed in the present study and the shorter rectangular bars studied by Nakagawa et al. [7]. The proximity of the present cylinder to the plane wall or free surface and differences in blockage are other possible reasons for the differences. A vortex formation length L_f is defined as the downstream location of the cylinder where the streamwise velocity fluctuation level has grown to a maximum [7]. A value of $L_f/D \approx 1.2$ was obtained for the present study and the circular cylinder. In their study, Nagakawa et al. [7] reported values of $L_f/D = 0.7$, 0.8, 1, and 2, respectively,

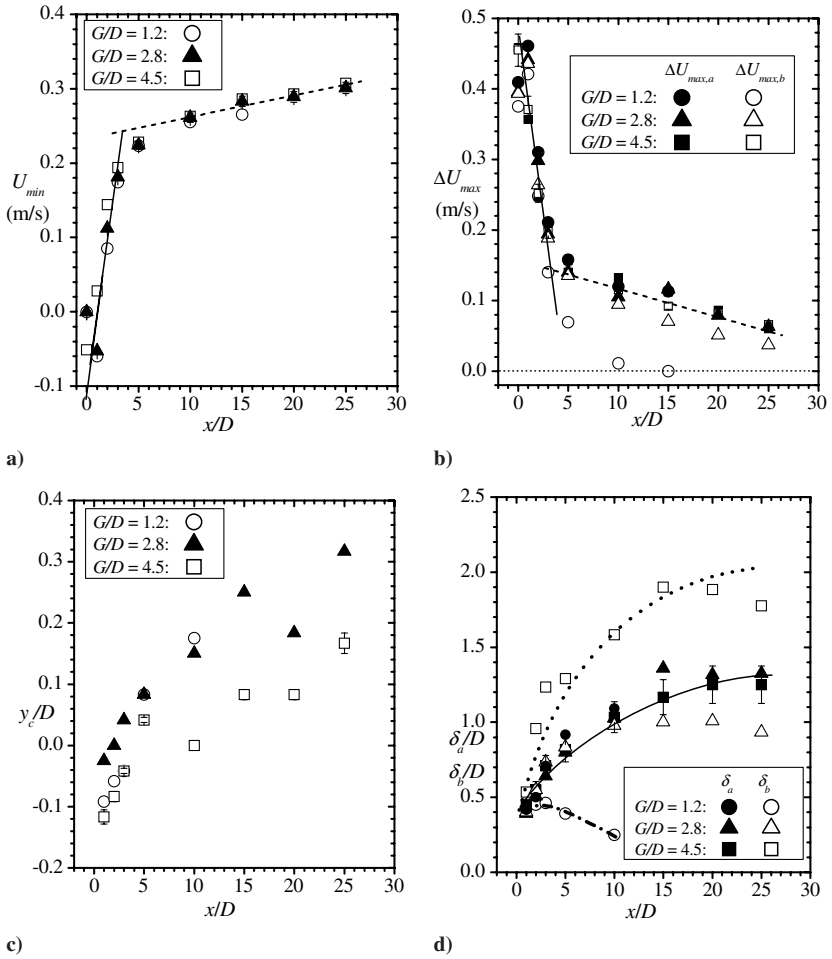

Fig. 7 The variation of a) the local minimum velocity, $U_{\min}$; b) maximum velocity difference, $\Delta U_{\max}$; c) location of the $U_{\min}$, y_c; and d) wake half-width above (δ_a) and below (δ_b) the wake axis with x.

for rectangular cylinders with $L/D = 0.5$, 1, 2, and 3. It should be noted that in all these studies, the difference between L_r and L_f is $0.2D$ or less.

2. *Variation of Wake Width with Streamwise Distance*

The shear layer growth is often characterized by the wake half-width which is defined as the y location where the mean velocity defect ($U_e - U$) decays to 50% of the maximum value as one moves away from the wake centerline ($y = 0$). For a cylinder in an infinite medium, U_e is constant (i.e., independent of x) but in the present study, the local maximum varied with x because of the proximity of the cylinder to the plane wall and/or free surface. Furthermore, at a given x location, the maximum velocities outside the lower and upper wake are different. The variation of $U_{\min}$ with x shows no distinct dependence on the gap ratio (Fig. 7a). The figure shows that $U_{\min}$ increased rapidly in the very near wake region: $x/D \leq 3$ ($U_{\min} = -0.177 + 0.124x/D$) than in the intermediate wake region: $10 \leq x/D \leq 25$ ($U_{\min} = 0.232 + 0.0029x/D$). Consequently, the maximum velocity difference, $\Delta U_{\max,a} = U_{\max,a} - U_{\min}$ and $\Delta U_{\max,b} = U_{\max,b} - U_{\min}$ (Fig. 7b) decayed more rapidly in the very near wake region $x/D \leq 3$ ($\Delta U_{\max} = 0.50 - 0.11x/D$ than further downstream: $5 \leq x/D \leq 25$ ($\Delta U_{\max} = 0.16 - 0.004x/D$). Note that when the cylinder is mounted close to the plane wall, $\Delta U_{\max,b}$ values decayed the most rapidly and became nearly zero for $x/D \geq 10$. For the intermediate gap ratio, $\Delta U_{\max,b}$ values are smaller than $\Delta U_{\max,a}$ values in the region $x/D \geq 10$ but the differences between $\Delta U_{\max,a}$ and $\Delta U_{\max,b}$ values are not as dramatic as observed for $G/D = 1.2$. As shown in Fig. 7c, the exact location of $U_{\min}$ tends to move away from the wake centerline and toward the free surface.

In the present study, the half-width of the wake above the wake axis, δ_a, is defined as the y location where $(U_{\max,a} - U)/(U_{\max,a} - U_{\min}) = 0.5$ as one moves from the wake axis toward the free surface while that below the wake axis, δ_b, is the y location where $(U_{\max,b} - U)/(U_{\max,b} - U_{\min}) = 0.5$ as one moves from the wake axis toward the plane wall. Figure 7d demonstrates the profound effects of the plane wall and the free surface on the variation of the wake half-widths with downstream distance. In general, the wake half-widths are the largest when the cylinder is mounted close to the free surface

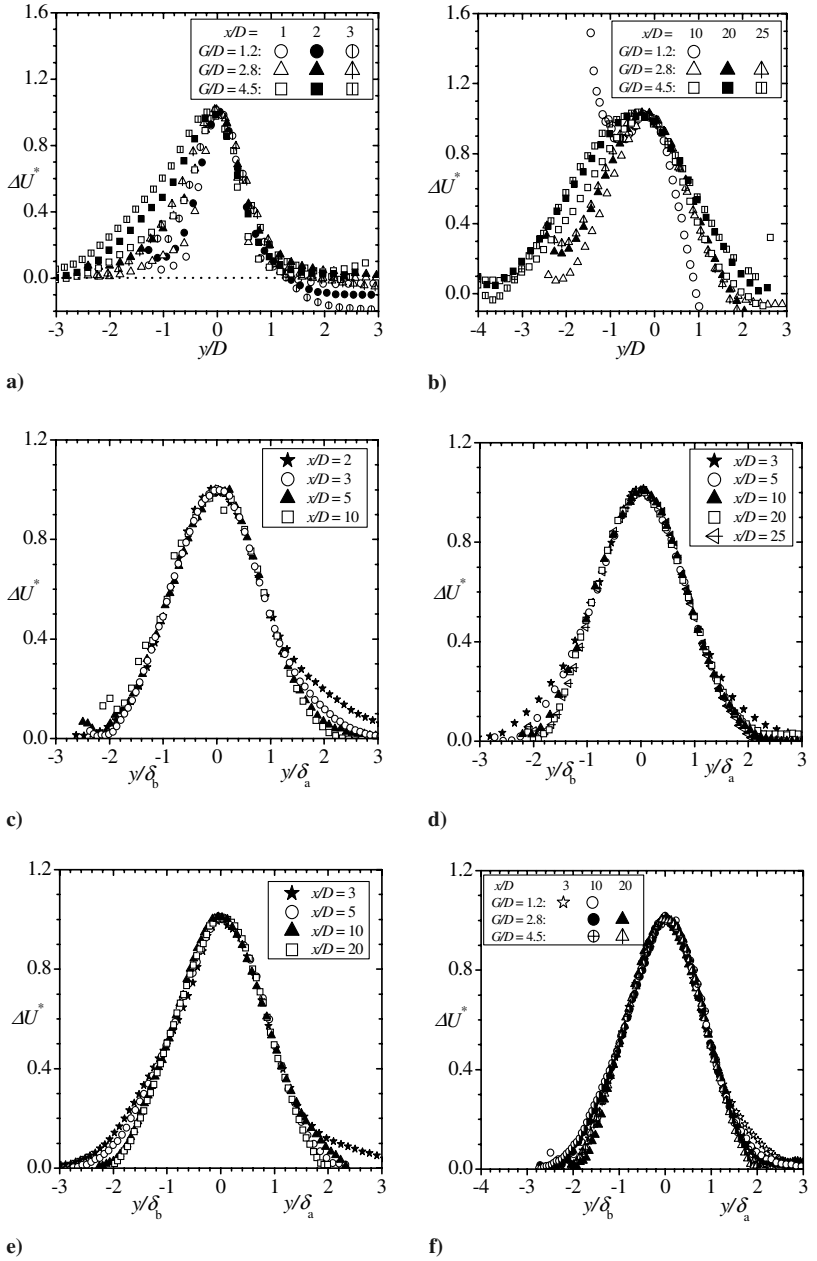

Fig. 8 The streamwise mean velocities across the wake at selected streamwise locations (x) as shown on each plot. Note the $\delta_a = y$ location where $(U_{\max,a} - U)/(U_{\max,a} - U_{\min}) = 0.5$ and $\delta_b = y$ location where $(U_{\max,a} - U)/(U_{\max,a} - U_{\min}) = 0.5$.

and the least when the cylinder is mounted close to the plane wall. For the intermediate gap ratio ($G/D = 2.8$), values of δ_a and δ_b are nearly the same up to $x/D = 10$, and this observation is consistent with the symmetric recirculation zones noted in Figs. 5c and 5d. Thereafter, the plane wall caused values of δ_b to become somewhat lower. The most dramatic effects are evident when the cylinder is mounted close to the plane wall ($G/D = 1.2$) or near the free surface ($G/D = 4.5$). For $G/D = 1.2$, δ_b decayed very rapidly while values of δ_a collapsed with those obtained for the intermediate gap ratio. This demonstrates that the plane wall suppressed the growth of the lower wake and at $x/D = 10$, δ_b is only 25% of the corresponding δ_a value. In the intermediate wake region, δ_a values for $G/D = 4.5$ are about 35% lower than the corresponding values obtained below the wake axis (δ_b).

3. *Mean Velocities and Turbulent Quantities Across the Wake*

The normalized mean velocity defect profiles across the wake at selected x/D are shown in Fig. 8. Figures 8a and 8b show plots for the three gap ratios in the near wake ($x/D \leq 3$) and intermediate wake ($x/D \geq 10$), respectively. In these plots, y is made dimensionless by the cylinder thickness, and the velocity difference is non-dimensionalized by the average of the maximum mean velocity above and below the wake axis. In these and subsequent plots, appropriate intermediate data points are skipped for clarity. As the flow develops downstream of the cylinder, it entrains the ambient fluid and the wake becomes wider. It should be noted that the profiles are not exactly symmetrical due to the effects of the plane wall or the free surface, and in the near wake region, departure from symmetry is more severe for $G/D = 1.2$ and 4.5 compared to $G/D = 2.8$. At $x/D \geq 10$ (Fig. 8b), the bottom (or left) half of the wake for $G/D = 1.2$ almost disappeared due to the strong interaction between the wake and the plane wall.

Profiles at selected locations (both in the near and intermediate wake regions) for $G/D = 1.2$ are plotted in Fig. 8c. In this plot, the bottom half is normalized by $U_{\max,b}$ and δ_b while the upper half is normalized by $U_{\max,a}$ and δ_a. With this scaling, it is seen that the two halves of the profiles are nearly symmetrical. The profiles obtained at the various x/D also collapse reasonably well in the region: $-1.3 < y/\delta < 1.3$. Similar scaling is used to plot data obtained for $G/D = 2.8$ and 4.5, respectively, in Figs. 8d and 8e, and it is observed that these profiles also collapsed onto each other. Figure 8f demonstrates that profiles obtained for the three gap ratios are nearly indistinguishable in the region $-1.3 < y/\delta < 1.3$. It should be remarked that a similar scaling was used to collapse profiles obtained in shallow wakes behind a flat plate over smooth and rough surfaces

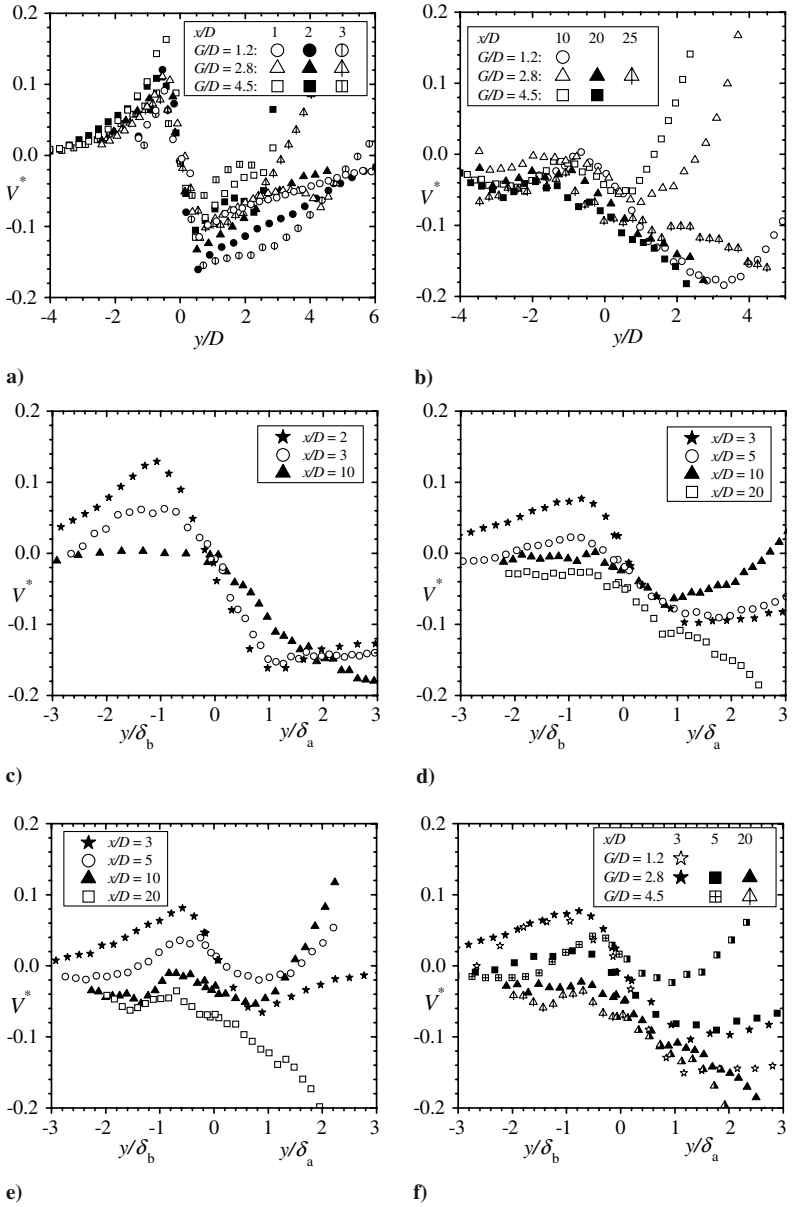

Fig. 9 The transverse mean velocities across the wake at selected streamwise locations (x) as shown on each plot.

[20], and also downstream of rectangular cylinders mounted vertically on the floor of the open channel [28]. The ability of this scaling to collapse the mean profiles in both the near and intermediate wake regions and also for all three gap ratios (Figs. 8c–8f) is remarkable because even for wake flow in an infinite medium, self-similarity is achieved only in the far wake region if classical scaling is used.

Figure 9a shows that in the near wake, the mean transverse velocity profiles are asymmetric about the wake axis. The values of V are predominantly positive for $y < 0$ and negative for $y > 0$. Below the wake axis ($y < 0$), the peak values decrease with increasing distance. At similar x/D locations, the peak values increase with G/D and the y location where $V = 0$ increases with G/D. This implies that, in the near wake region, entrainment of ambient fluid into the lower wake region is higher for the higher G/D (when the cylinder is mounted close to the free surface). Above the wake axis, on the other hand, the magnitude of V and region of negative V increase with decreasing G/D. In the intermediate wake, V is predominantly negative (even below the wake axis) and the magnitude of V decreased in comparison to values found in the near wake region.

The profiles of streamwise turbulence intensity show the expected double peak (Fig. 10). At $x/D = 1$, they are nearly symmetric about the wake axis. In the near wake region, the peak value increases with x/D, irrespective of the gap ratio which implies that in this region $U_{max} - U_{min}$ decayed more rapidly than u_{max} did. The effects of the plane wall on the profiles for $G/D = 1.2$ can be seen from the significant reduction of the left peak at $x/D = 2$ and 3, and at $x/D = 10$, no distinct peak is observed below the wake axis. The free surface also tends to reduce the peak above the wake axis for $G/D = 4.5$ notwithstanding the high background turbulence level close to the free surface. The profiles for the intermediate gap ratio are nearly symmetrical about the wake axis. Figure 11 shows that, unlike the streamwise turbulent intensity, the peak values of the transverse turbulent intensity profiles occurred on the wake axis. In the near wake region, v^*_{max} also tends to increase with x/D for all gap ratios but in the intermediate wake region, v^*_{max} remains nearly constant for $G/D = 2.8$ and 4.5.

The Reynolds shear stress is antisymmetric about the wake axis (Fig. 12) in conformity with the shear layer. There is a substantial increase in $-uv^*$ with increasing downstream distance. Below the wake axis, profiles for $G/D = 1.2$ decayed to zero more rapidly than the larger gap ratios while above the wake axis, profiles for $G/D = 4.5$ decayed to zero more rapidly than for the lower gap ratios. For the intermediate gap ratio ($G/D = 2.8$, Fig. 12d), the peak values above and below the wake axis are nearly the same at all locations. The profiles at various axial locations also collapsed reasonably well in the vicinity of the wake axis. For the smallest gap ratio, the left and right peak values are similar in the near wake region while in the intermediate wake region the plane wall reduced the left peak in

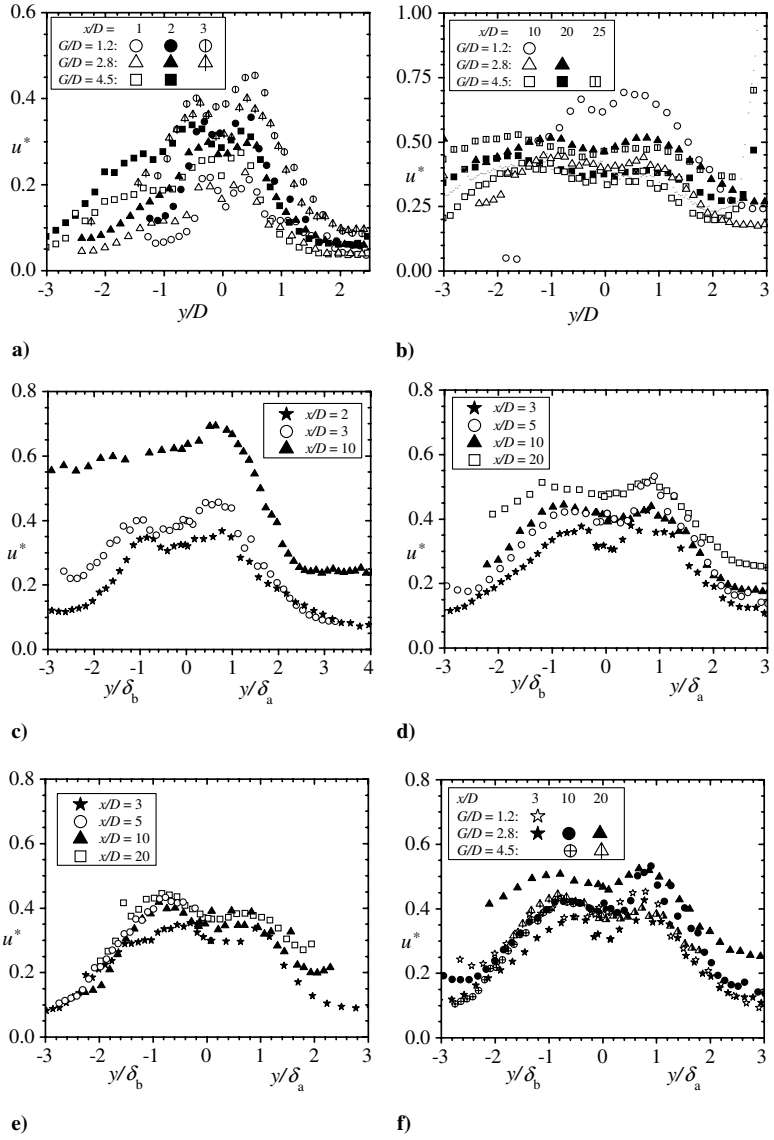

Fig. 10 The streamwise turbulent intensities across the wake at selected streamwise locations (x) as shown on each plot.

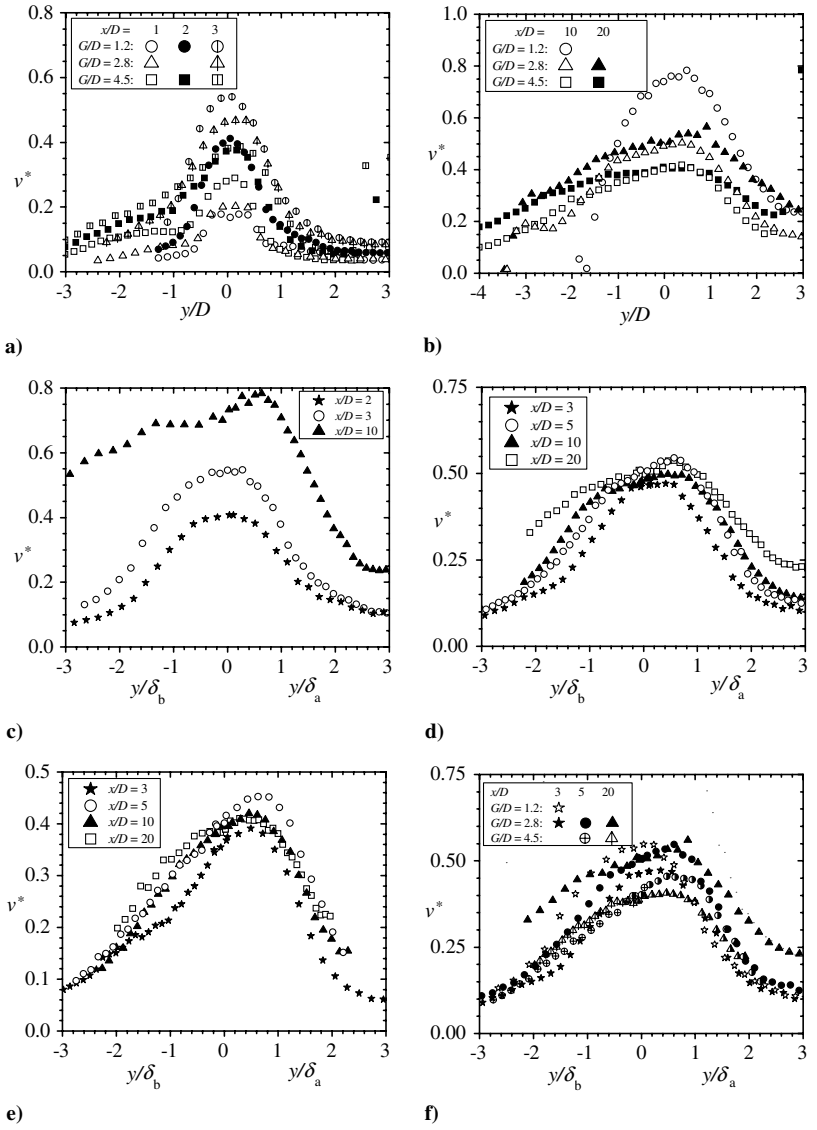

Fig. 11 The transverse turbulent intensities across the wake at selected streamwise locations (x) as shown on each plot.

comparison to the right peak. For the largest gap ratio, the lower peaks are typically larger than corresponding values above the wake axis.

IV. Conclusions

The results presented in this paper showed that the plane wall decreased the magnitude of $(U/U_e)_{\min}$ along the wake axis by 25% compared to the value measured for the intermediate cylinder location whereas the free surface increased the magnitude of $(U/U_e)_{\min}$ by 20%. It was found that the variation of the turbulent quantities along the wake axis was not significantly affected by the cylinder's proximity to the plane wall and free surface. The present data showed that the transverse turbulent intensity was substantially higher than the streamwise turbulent intensity. The turbulence levels measured along the wake axis in the present work were significantly lower than values reported for square and circular cylinders whereas the length of the mean recirculation zone was found to be similar to values reported in prior circular cylinder experiments but higher than those reported for a square cylinder.

For the intermediate cylinder location, the flow patterns as well as the profiles of the mean velocities and the turbulent quantities, and the wake half-widths were nearly symmetric about the wake axis. It was observed that the effects of the plane wall and the free surface on the separated shear layer and wake downstream of a rectangular cylinder in an open channel were qualitatively similar. This is based on the premise that the plane wall tends to reduce the size of the recirculation zone closer to the plane wall while the free surface suppresses the recirculation zone closer to the free surface. When the cylinder was mounted close to the plane wall, the lower half of the wake was suppressed and eventually annihilated beyond 10 cylinder thicknesses downstream of the trailing edge because of the strong interaction with the plane wall. The plane wall also attenuated the spread of the lower half of the wake substantially whereas the free surface reduced the spread of the upper half of the wake compared to values obtained for the lower half of the wake. For example, when the cylinder is mounted close to the plane wall, the half-width of the lower wake at $x/D = 10$ was only 25% of the corresponding value for the upper wake. On the other hand, when the cylinder was mounted close to the free surface, the half-width of the upper wake in the intermediate wake region was about 35% lower than the corresponding values for the lower wake. Notwithstanding these qualitative similarities, it was observed that the half-widths were significantly larger when the cylinder was mounted close to the free surface than when it was mounted close to the plane wall. Unlike classical scaling, the mean velocity defect profiles across the wake showed a sense of similarity in the near and intermediate wake regions when the local wake half-width and maximum velocity were

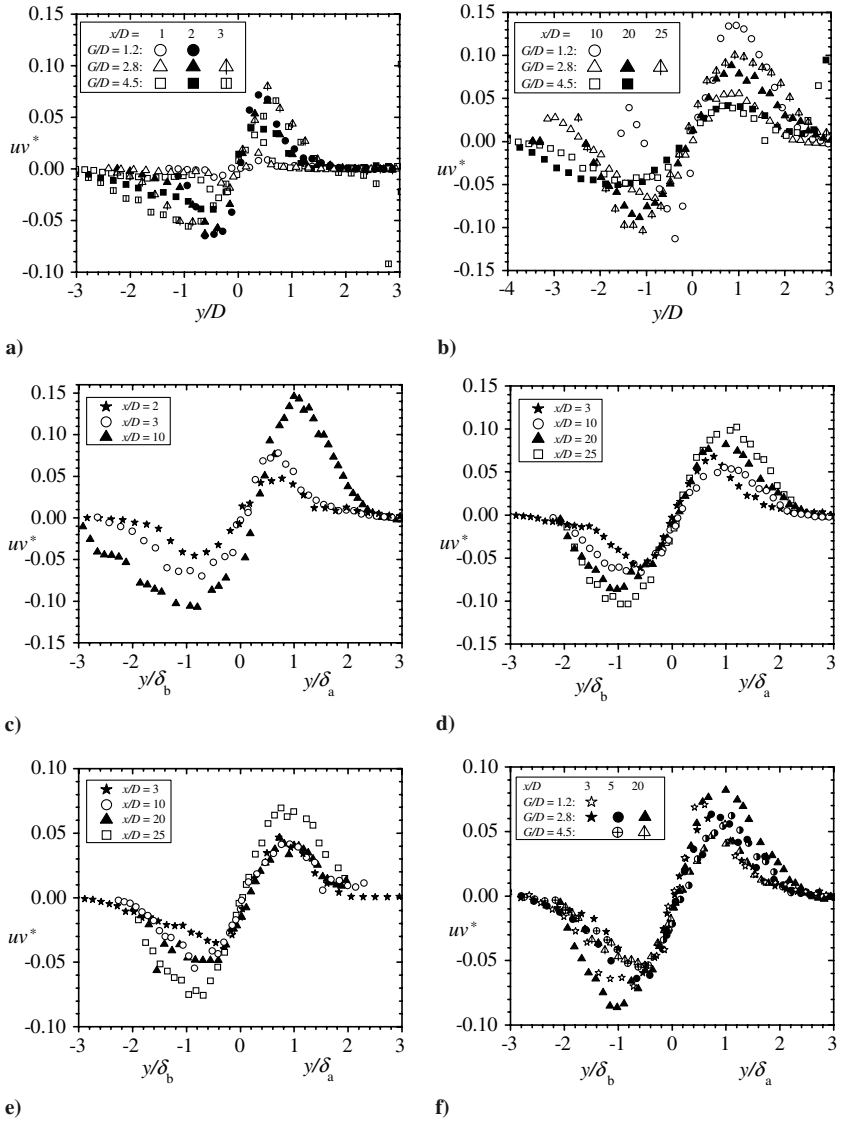

Fig. 12 The Reynolds shear stress across the wake at selected streamwise locations (x) as shown on each plot.

used as the appropriate length and velocity scales for the upper and lower halves of the wake. This scaling was, however, less successful in collapsing the turbulent quantities.

References

[1] Berger, E., and Wille, R., "Periodic Flow Phenomena," *Annual Review of Fluid Mechanics*, Vol. 4, Jan. 1972, pp. 313–340. doi:10.1146/annurev.fl.04.010172.001525

[2] Williamson, C. H. K., "Oblique and Parallel Modes of Vortex Shedding in the Wake of a Circular Cylinder at Low Reynolds Numbers," *Journal of Fluid Mechanics*, Vol. 206, 1989, pp. 579–627. doi:10.1017/S0022112089002429

[3] Catalano, P., Wang, M., Iaccarino, G., and Moin, P., "Numerical Simulation of the Flow Around a Circular Cylinder at High Reynolds Numbers," *International Journal of Heat and Fluid Flow*, Vol. 24, No. 4, 2003, pp. 463–469. doi:10.1016/S0142-727X(03)00061-4

[4] Nakamura, Y., Ohya, Y., and Tsuruta, H., "Experiments on Vortex Shedding from Flat Plates with Square Leading and Trailing Edges," *Journal of Fluid Mechanics*, Vol. 222, Jan. 1991, pp. 437–447. doi:10.1017/S0022112091001167

[5] Lyn, D. A., Einav, S., Rodi, W., and Park, J. H., "A Laser-Doppler Velocimetry Study of Ensemble-Averaged Characteristics of the Turbulent Near Wake of a Square Cylinder," *Journal of Fluid Mechanics*, Vol. 304, Dec. 1995, pp. 285–319. doi:10.1017/S0022112095004435

[6] Durao, D. F. G., Heitor, M. V., and Pereira, J. C. F., "Measurements of Turbulent and Periodic Flows Around a Square Cross-Section Cylinder," *Experiments in Fluids*, Vol. 6, No. 5, 1988, pp. 298–304. doi:10.1007/BF00538820

[7] Nakagawa, S., Nitta, K., and Senda, M., "An Experimental Study on Unsteady Turbulent Near Wake of a Rectangular Cylinder in a Channel Flow," *Experiments in Fluids*, Vol. 27, No. 3, 1999, pp. 284–294. doi:10.1007/s003480050353

[8] Matsumara, M., and Antonia, R., "Momentum and Heat Transfer in the Turbulent Intermediate Wake of a Circular Cylinder," *Journal of Fluid Mechanics*, Vol. 250, May 1993, pp. 277–296. doi:10.1017/S0022112093001466

[9] Taneda, S., "Experimental Investigation of Vortex Streets," *Journal of the Physical Society of Japan*, Vol. 20, No. 9, 1965, pp. 1714–1721.

[10] Price, S. J., Sumner, D., Smith, J. G., Leong, K., and Paidoussis, M. P., "Flow Visualization Around a Circular Cylinder Near to a Plane Wall," *Journal of Fluids and Structures*, Vol. 16, No. 2, 2002, pp. 175–191. doi:10.1006/jfls.2001.0413

[11] Bearman, P. W., and Zdravkovich, M. M., "Flow Around a Circular Cylinder Near a Plane Boundary," *Journal of Fluid Mechanics*, Vol. 89, Nov. 1978, pp. 33–47. doi:10.1017/S002211207800244X

[12] Zdravkovich, M. M., "Forces on a Circular Cylinder Near a Plane Wall," *Applied Ocean Research*, Vol. 7, No. 4, 1985, pp. 197–201. doi:10.1016/0141-1187(85)90026-4

[13] Taniguchi, S., and Miyakoshi, K., "Fluctuating Fluid Forces Acting on a Circular Cylinder and Interference with a Plane Wall," *Experiments in Fluids*, Vol. 9, No. 4, 1990, pp. 197–204. doi:10.1007/BF00190418

[14] Lei, C., Cheng, L., and Kavanagh, K., "Re-Examination of the Effect of a Plane Boundary on Force and Vortex Shedding of a Circular Cylinder," *Journal of Wind Engineering and Industrial Aerodynamics*, Vol. 80, No. 3, 1999, pp. 263–286. doi:10.1016/S0167-6105(98)00204-9

[15] Dipankar, A., and Sengupta, T. K., "Flow Past a Circular Cylinder in the Vicinity of a Plane Wall," *Journal of Fluids and Structures*, Vol. 20, No. 3, 2005, pp. 403–423. doi:10.1016/j.jfluidstructs.2005.01.001

[16] Reichl, P., Hourigan, K., and Thompson, M. C., "Flow Past a Cylinder Close to a Free Surface," *Journal of Fluid Mechanics*, Vol. 533, June 2005, pp. 269–296.

[17] Ingram, G. R., and Chu, V. H., "Flow Around Islands in Rupert Bay: An Investigation of the Bottom Friction Effect," *Journal of Geophysical Research*, Vol. 92, No. C13, 1987, pp. 14,521–14,533.

[18] Ramachandran, S., "Velocity and Concerntration Measurement in Shallow Turbulent Near Wakes," M.Sc. Thesis, University of Saskachewan, Canada, 1998.

[19] Balachandar, R., Tachie, M. F., and Chu, V. H., "Concerntration Measurement in Intermediate Shallow Wakes," *Journal of Fluids Engineering*, Vol. 121, No. 1, 1999, pp. 34–43.

[20] Tachie, M. F., and Balachandar, R., "Shallow Wakes Generated on Smooth and Rough Surfaces," *Experiments in Fluids*, Vol. 30, No. 4, 2001, pp. 467–474. doi:10.1007/s003480000228

[21] Coleman, H. W., and Steele, W. G., "Engineering Application of Experimental Uncertainty Analysis," *AIAA Journal*, Vol. 33, No. 10, 1995, pp. 1888–1896.

[22] Prasad, A. K., Adrian, R. J., Landreth, C. C., and Offutt, P. W., "Effect of Resolution on the Speed and Accuracy of Particle Image Velocimetry Interrogation," *Experiments in Fluids*, Vol. 13, Nos. 2–3, 1992, pp. 105–116. doi:10.1007/BF00218156

[23] Forliti, D. J., Strykowski, P. J., and Debatin, K., "Bias and Precision Errors of Digital Particle Image Velocimetry," *Experiments in Fluids*, Vol. 28, No. 5, 2000, pp. 436–447. doi:10.1007/s003480050403

[24] Tachie, M. F., Agelinchaab, M., and Shah, M. K., "Turbulent Flow over Transverse Ribs in Open Channel with Converging Side Walls," *International Journal of Heat and Fluid Flow*, Vol. 28, No. 4, 2006, pp. 683–707.

[25] Agelinchaab, M., and Tachie, M. F., "Open Channel Turbulent Flow over Hemispherical Ribs," *International Journal of Heat and Fluid Flow*, Vol. 27, No. 6, 2006, pp. 1010–1027. doi:10.1016/j.ijheatfluidflow.2006.03.001

[26] Hermann, F., Billeter, R., and Hollenstein, R., "Investigation of the Flow Through a Trashrack Under Different Inflow Condition," *Hydroinformatics, '98*, Balkema, Rotterdam, 1998, pp. 121–128.

[27] Paul, S. S., "Experimental and Numerical Study of Turbulent Cross-Flow in a Staggered Tube Bundle," Ph.D. Thesis, University of Manitoba, Canada, 2006.

[28] Balachandar, R., and Tachie, M. F., "A Study of Boundary Layer-Wake Interaction in Shallow Open Channel Flows," *Experiments in Fluids*, Vol. 30, No. 5, 2001, pp. 511–521. doi:10.1007/s003480000230

F. Coton
Associate Editor